Chemical Engineering Journal 471 (2023) 144464

Contents lists available at ScienceDirect

Chemical Engineering Journal

journal homepage: www.elsevier.com/locate/cej

Facile synthesis of visible-responsive photocatalytic Eu-doped layered double hydroxide for selective removal of NO_x pollutant

Adrián Pastor [a,*], Chunping Chen [b], Gustavo de Miguel [c], Francisco Martín [d], Manuel Cruz-Yusta [a], Dermot O'Hare [b], Ivana Pavlovic [a], Luis Sánchez [a,*,1]

[a] Departamento de Química Inorgánica, Instituto de Química para la Energía y Medioambiente, Universidad de Córdoba, Campus de Rabanales, E-14014 Córdoba, Spain
[b] Chemistry Research Laboratory, Department of Chemistry, University of Oxford, Oxford OX1 3TA, UK
[c] Departamento de Química Física y Termodinámica Aplicada, Instituto de Química para la Energía y Medioambiente, Universidad de Córdoba, Campus de Rabanales, E-14014 Córdoba, Spain
[d] Departamento de Ingeniería Química, Facultad de Ciencias, Universidad de Málaga, Campus de Teatinos, E-29071 Málaga, Spain

ARTICLE INFO

Keywords:
LDH
Photocatalyst
Nitrogen oxides
Europium
Visible light

ABSTRACT

Efficient nitrogen oxides (NO_x) removal from the urban atmosphere is still a target for the researchers. Herein, a Zn_2Al-CO_3 based layered double hydroxide (LDH) was doped with increasing amounts of Eu^{3+} (0.01–0.04) and the photocatalytic oxidation of NO_x gases was investigated. The LDHs were synthesized by a facile coprecipitation method at room temperature and ambient pressure. The successful Eu^{3+} substitution in the LDH layers induces a shift in the M−O bonds that modifies the electronic band structure of the doped photocatalysts. Compared to the undoped LDH, the NO_x removal efficiency was enhanced by ~ 17–25 % under UV–Vis light irradiation. Remarkably, a NO_x removal efficiency of ~ 47 % was attained by the optimally doped LDH under Visible irradiation (420 nm), surpassing raw LDH (~ 9 %). Moreover, the Eu^{3+} doped LDHs retained its photocatalytic efficiency during long periods of irradiation during consecutive tests with high selectivity (>90 %). Photoluminescence studies indicated that Eu^{3+} was located in a non-centrosymmetric position, thereby producing structural disorder within the lattice. Eu doping promoted charge separation and a higher production of ·OH radicals as verified by time-resolved photoluminescence and electron paramagnetic resonance, respectively. We believe this work reports unprecedent results obtained by Eu-doping of Zn_2Al-based LDHs under visible light for NO_x photooxidation and serves as a new strategy to prepare functional LDHs for other photocatalytic applications.

1. Introduction

Layered Double Hydroxides (LDHs) are a class of layered compounds which possesses a brucite-like structure. The layers have positive charge due to the substitution of divalent metal cations (M^{z+}) by tri or tetravalent metal cations (M'^{y+}), this charge is balanced by intergallery anions (A^{n-}) embedded between the brucite-like sheets [1,2]. LDHs have the formula $[(M^{z+}_{1-x}M'^{y+}_{x}(OH)_2)^{w+}](A^{n-})_{w/n}{\cdot}mH_2O$, giving rise to enormous composition possibilities. The unique LDH structural features, together with its 2D morphology, bandgap engineering, diverse electronic excitation pathways, highly dispersion of metal sites, low cost, or facile synthesis have attracted a recent interest in the field of photocatalysis [3,4]. In this context, LDHs have acquired application prospects in CO_2 photoreduction [5,6], water splitting [7], nitrogen reduction [8] and photodegradation of organic pollutants [9].

Remarkably, a recent application for the LDHs consists in the photocatalytic removal of NO_x gases from the urban environment (De-NO_x process) [10–14]. In this methodology, the LDH photocatalyst can oxidize NO_x towards nitrates/nitrites species thanks to the interaction of water, oxygen, and sunlight irradiation from the atmosphere [14,15]. Notwithstanding the latest progresses in LDHs as De-NO_x photocatalysts, typically LDHs show poor De-NO_x performance under visible light irradiation due to a high recombination ratio of the photocharges, thereby limiting the efficiency for the solar energy harvesting [10,11,13,16]. Generally, LDH photocatalysts usually require the combination with other non-sustainable compounds (e.g., quantum dots,

* Corresponding authors.
E-mail addresses: q92paesa@uco.es (A. Pastor), luis-sanchez@uco.es (L. Sánchez).
[1] ORCID ID: 0000-0002-0194-1908

https://doi.org/10.1016/j.cej.2023.144464
Received 29 April 2023; Received in revised form 19 June 2023; Accepted 26 June 2023
Available online 27 June 2023
1385-8947/© 2023 The Author(s). Published by Elsevier B.V. This is an open access article under the CC BY-NC-ND license (http://creativecommons.org/licenses/by-nc-nd/4.0/).

noble metal nanoparticles, Bi-containing compounds, etc.) to overcome its limited visible-light photocatalytic performance [17–21]. In this context, LDH doping is an excellent way for tailoring the band gap energy, allowing improvements in light absorption and carrier separation.

Doping photocatalysts with Eu^{3+} cations has been a common approach in many photocatalytic applications because the rich electron availability and the numerous electron transitions in the Eu 4*f* orbitals, thus favoring photocharge migration. Furthermore, owing to its large cationic radius (0.95 Å), Eu^{3+} insertion into a lattice structure may create strain or defects, which can produce new energetic states in the band gap of the material, serving as new ways for photocharge deactivation and thus improving the photocatalytic performance [22,23]. In this sense, ZnO [24–26], TiO_2 [22,27–29], Bi-containing compounds [30,31] or $CaWO_4$ [32] have been doped with Eu^{3+} to obtain improvements in visible light response, retardation in electron-hole recombination or increasing absorption edge.

Herein, we have doped Zn_2Al-LDH with small quantities of Eu^{3+} by using a coprecipitation method at room temperature. Eu doping, by various amounts, was carried out by partial replacement of Al^{3+} in the metal hydroxide layers of the LDH. Changes in the crystalline structure, light absorption ability and electronic properties were observed for the europium containing Zn_2Al-LDH samples. Photoluminescence and spin-trapping experiments revealed that the optimal Eu-doped LDH had less photocharge recombination and higher radicals production. As a result, the Zn_2AlEu_x-LDH samples ($x = 0.01$–0.04) exhibit higher performance for the photochemical abatement of NO_x gases, specially under visible light irradiation. To the best of our knowledge, this work reports for the first time the use of Eu-doped LDHs as photocatalysts, these materials exhibit unprecedent performance efficiencies for De-NO_x under visible light, opening the door to new research in the field of photocatalytic systems based on LDHs.

2. Materials and methods

2.1. Chemicals

The following raw chemicals were used as received from Sigma-Aldrich: $ZnCl_2$, $AlCl_3{\cdot}6H_2O$, $EuCl_3$, Na_2CO_3, NaOH, methanol and 5,5-dimethyl-l-pyrroline-N-oxide (DMPO). Milli-Q® water was used for the experimental section.

2.2. Photocatalysts preparation

A modified method from the literature was adopted in order to synthesize the Eu-doped Zn_2Al-LDHs [33]. Solution A was prepared by dissolving 60 mmol NaOH and 20 mmol Na_2CO_3 in 80 mL H_2O. Solution B was prepared by dissolving 20 mmol $ZnCl_2$, *a* mmol $AlCl_3{\cdot}6H_2O$, and *b* mmol $EuCl_3$ in 80 mL H_2O ($a + b = 10$ mmol). The Zn^{2+}:M^{3+} ratio was kept to 2 and the Eu^{3+}:($Al^{3+} + Eu^{3+}$) molar ratio (R) was varied ($R = [b/(a+b)] \times 100 = 0$, 2, 10 or 15). Solution A was thoroughly dropped into solution B by using a syringe pump (1.86 mL min^{-1}) under vigorous magnetic stirring (1000 rpm). After that, the mixture was aged at room temperature for 24 h, keeping the magnetic stirring at 500 rpm. Subsequently, the dispersion was centrifugated (4000 rpm, 5 min) and washed with water several times, until pH = 7. Finally, the obtained LDH was dried in a vacuum oven at 30 °C for 24 h, obtaining around 3 g of a white powder. The sample nomenclature was Zn_2Al (no doping; R = 0) or Zn_2AlEu-R (Eu doping), R indicated the above-mentioned molar ratio. It is worth mentioning that the Zn^{2+}:M^{3+} ratio influences the photocatalytic efficiency [12]. However, even though the identical synthesis protocol was essayed, other attempts with different metal ratio failed. Thus, by using a Zn^{2+}:($Al^{3+} + Eu^{3+}$) ratio = 3, impure LDH was obtained (extra phase of ZnO was found).

2.3. Characterization of the samples

The obtained samples were characterized using the following techniques: Synchrotron X-ray diffraction (SXRD), X-ray photoelectron spectra (XPS), Ultraviolet Photoelectron Spectroscopy (UPS), Attenuated total reflectance Fourier transform infrared spectroscopy (ATR-FT-IR), in situ diffuse reflectance infrared Fourier transform spectra (DRIFTS), Raman spectroscopy, Ultraviolet–Visible Diffuse Reflectance Spectroscopy (UV–Vis DRS), Nitrogen adsorption–desorption isotherms; High Resolution Transmission Electron Microscopy (HRTEM), Scanning Electron Microscopy (SEM), Energy Dispersive X-ray spectroscopy (EDX), X-Ray Fluorescence (XRF), Thermogravimetric analysis (TGA), steady-state photoluminescence spectroscopy (PL), Time-Resolved Photoluminescence spectroscopy (TRPL); Electron Paramagnetic Resonance (EPR). The $\Omega_{2,4}$ Judd-Ofelt parameters were experimentally determined from the PL emission spectra.

Further details can be found in "Electronic Supplementary Information" (SI).

2.4. Photocatalytic activity evaluation

The performance of the samples towards the photochemical oxidation of NO_x pollutants was assessed in a laminar flow reactor containing a 50 × 50 mm quartz sample holder (500 mg sample). The reactor was placed inside a sealed irradiation box (Solarbox 3000e RH with Xe lamp and controlled irradiance). Samples were irradiated during the tests with a UV–Vis Xe lamp (irradiances of 25 and 580 W m^{-2} for UV and visible light, respectively) or a visible light source (Light Emitting Diode of $\lambda = 420$ nm; 550 W m^{-2}). For each test, a gas mixture (NO and air) was constantly flowed (0.37 L min^{-1}; NO concentration = 150 ppb; mass flow controllers were used) into the reactor. The relative humidity was set to 50 ± 5 % by passing the air flow through a gas-washing bottle filled with demineralized water. The outlet gas was continuously measured by a chemiluminescence analyzer (Environment AC32M) to know the concentration of NO, NO_x and NO_2 gases. Before the irradiation period to start, adsorption − desorption equilibrium for the photocatalyst was completed upon passing the air/NO flow into the reactor in the dark for 10 min. A photocatalytic test blank (no sample on the sample holder) was performed to discard NO photolysis. Tests were repeated three times and the mean gas concentration values were calculated from triplicate experiments. The obtained standard deviations were ± 0.3 ppb for NO concentration and ± 1.0 ppb for NO_2 and NO_x concentrations. The following removal efficiency (E_{NO}, E_{NOx}) and selectivity (S) indexes were used to know about the photocatalytic performance of the samples during the light illumination period:

$$E_Z = (C_i - C_o) \times 100/C_i \quad (1)$$

$$S = (E_{NOx}/E_{NO}) \times 100 \quad (2)$$

where C_i and C_o represent the measured inlet and outlet concentrations and *z* the measured gas (NO or NO_x).

3. Results and discussion

3.1. Structural properties

Synchrotron X-ray diffraction (SXRD) patterns were collected to thoroughly determine the crystalline phases present and the structural parameters for the synthesized samples, Fig. 1A. All samples display patterns corresponding to the typical Bragg reflections for LDH compounds (JCPDS: 0048–1023; $3R_1$ polytype) [34], no impurity phases such as ZnO or Eu_2O_3 were observed. The low intensity Bragg reflections located at $2\theta \sim 17.9$, 27.4 and 29.2° were related to the presence of LDHs with $3R_2$ polytype [35]. The Eu insertion into the LDH structure led to a slight decrease in the crystallinity when compared to the

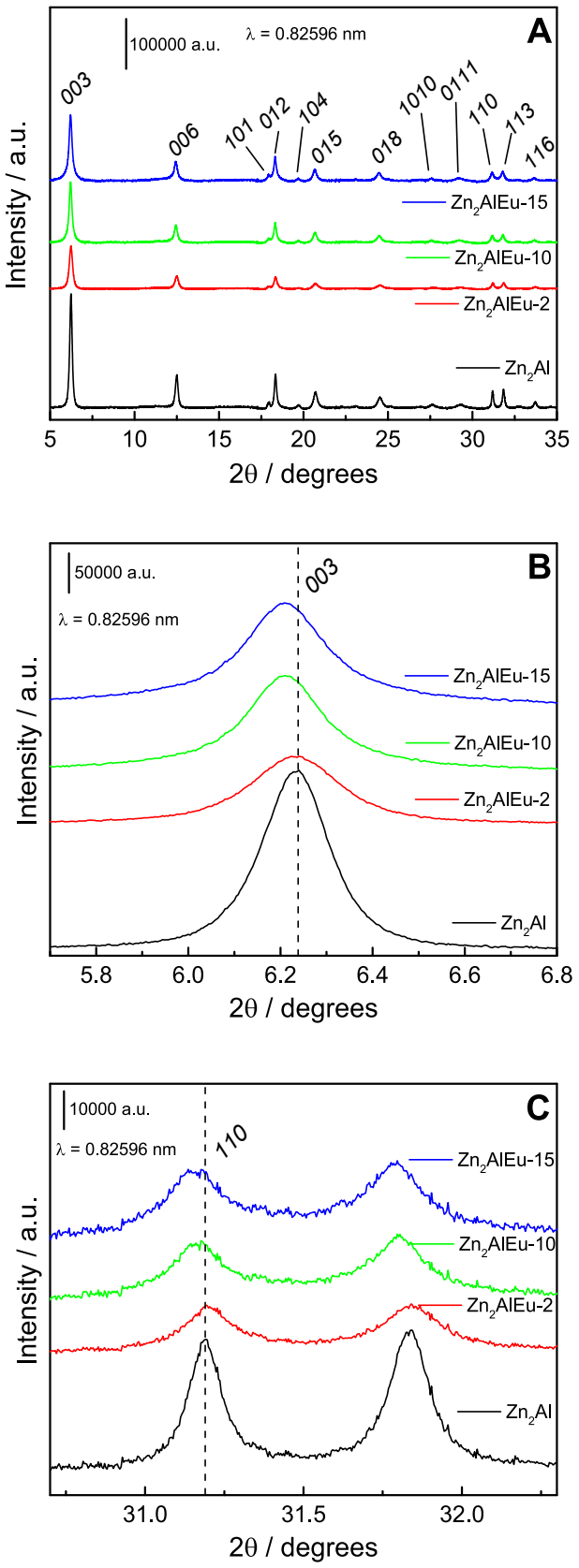

Fig. 1. (A) SXRD patterns of the synthesized LDHs and enlargements for: (B) *003* and (C) *110* Bragg reflections.

undoped Zn_2Al LDH. Possibly, the substitution of Al^{3+} (0.54 Å ionic radius) by the larger Eu^{3+} (0.95 Å) should produce distortions in the brucite-like sheets, limiting the growth of the LDH crystals [36]. The broadening of the reflections as the Eu amount increases can be quantified by use of the Scherrer equation, observing a general decrease in the crystalline domain length of the Eu-doped LDHs (Table 1). The basal spacing d_{003} for the LDHs was around 7.6 Å (Table 1), value associated to the presence of carbonate anion in the interlayer space. The lattice parameters of the LDHs were calculated from the SXRD [35]. A small but linear increase in the d_{003} spacing was observed with increasing Eu content, leading to higher *c* values (Fig. 1B and Table 1). This indicates that an increase in the thickness of the sheets may be caused by the successfully incorporation of Eu^{3+} into the LDH layers, as expected for lanthanide-containing LDHs [37]. Moreover, the *a* lattice parameter is equivalent to the mean metal–metal distance in the layers, which can be obtained from the position of the (*1 1 0*) Bragg reflection. In this regard, a slight displacement to lower 2θ degrees is also observed for this reflection (Fig. 1C), specially for the highest Eu doping level (Zn_2AlEu-15), which corresponds to an increase in the *a* lattice parameter following substitution of Al^{3+} by Eu^{3+} in the hexagonal cell (Table 1).

In the FT-IR spectra of the samples (Fig. 2A), the broad band located at ~ 3420 cm^{-1} is due to the O–H stretching vibration coming from both the water molecules and the OH^- from the metallic sheets; the shoulder at ~ 3044 cm^{-1} is due to the carbonate-water bridging mode in the interlayer [38]. The bands observed in the range between ~ 1560–1650 cm^{-1} belong to the O–H bending vibration of the water molecules [38,39]. The band located at 1496 cm^{-1}, whose intensity increases with the Eu content, must be caused by the ν_3 symmetric stretching vibration of lanthanide–carbonate, pointing to an interaction between Eu^{3+} cations on the hydroxide layers and the interlayer CO_3^{2-} anions [40]. The sharp band ascribed to CO_3^{2-} interlayer anion is positioned at ~ 1360 cm^{-1} (antisymmetric ν_3 mode). The small band appearing at 1050 cm^{-1}, only in the Zn_2AlEu-15 sample, corresponds to the deformation modes of the hydroxyl groups mainly influenced by the trivalent metals in the layers [41]. This suggests that the LDH with the highest Eu^{3+} content might experiment changes for the OH^- locations in the LDH framework. The bands below ~ 1000 cm^{-1} may be attributed to metal–oxygen and others carbonate vibration modes. Thus, in the 900–600 cm^{-1} region (Fig. 2B), the low intensity shoulders at ~ 862 and ~ 688 cm^{-1} are typical for vibrational modes (ν_4 and ν_2) of the interlayer carbonate anions in LDHs [38,42,43].

Barely appreciable bands located around 630 and 603 cm^{-1} can be ascribed to hydroxyl translation modes influenced by the di/tri-valent cations. Interestingly, an evident red-shift for the band at 765 cm^{-1} is observed as the Eu content increases in the LDH framework. This band arises from the translation modes of the OH^- groups mainly influenced by the trivalent cations [42] and, thereby, a higher presence of Eu^{3+} in the lattice seemed to increase the length of the M^{3+}–OH bonds. Additionally, a displacement of the O–H stretching vibration (3600 – 3100 cm^{-1} range; Fig. 2C) towards higher wavenumber is observed with the increased Eu content, indicating that M−OH interactions are also affected by the Eu doping. These band shifts are probably due to the lower polarizing effect of Eu^{3+} compared to that of Al^{3+} [38].

In order to further investigate the M−O interactions, Raman spectra were measured for all samples in the low-frequency range (Fig. S1). Four bands appeared at around 1060, 552, 495 and 152 cm^{-1} for all studied

Table 1
Calculated basal spacings and lattice parameters for the synthesized LDHs.

Sample	d_{003} (Å)	Lattice parameters (Å)		Crystal domain length (Å)	
		a	*c*	*c*-axis	*ab* plane
Zn_2Al	7.59	3.07	22.77	250.2	728.8
Zn_2AlEu-2	7.60	3.07	22.80	182.1	473.0
Zn_2AlEu-10	7.62	3.07	22.87	209.1	435.9
Zn_2AlEu-15	7.62	3.08	22.87	192.0	370.1

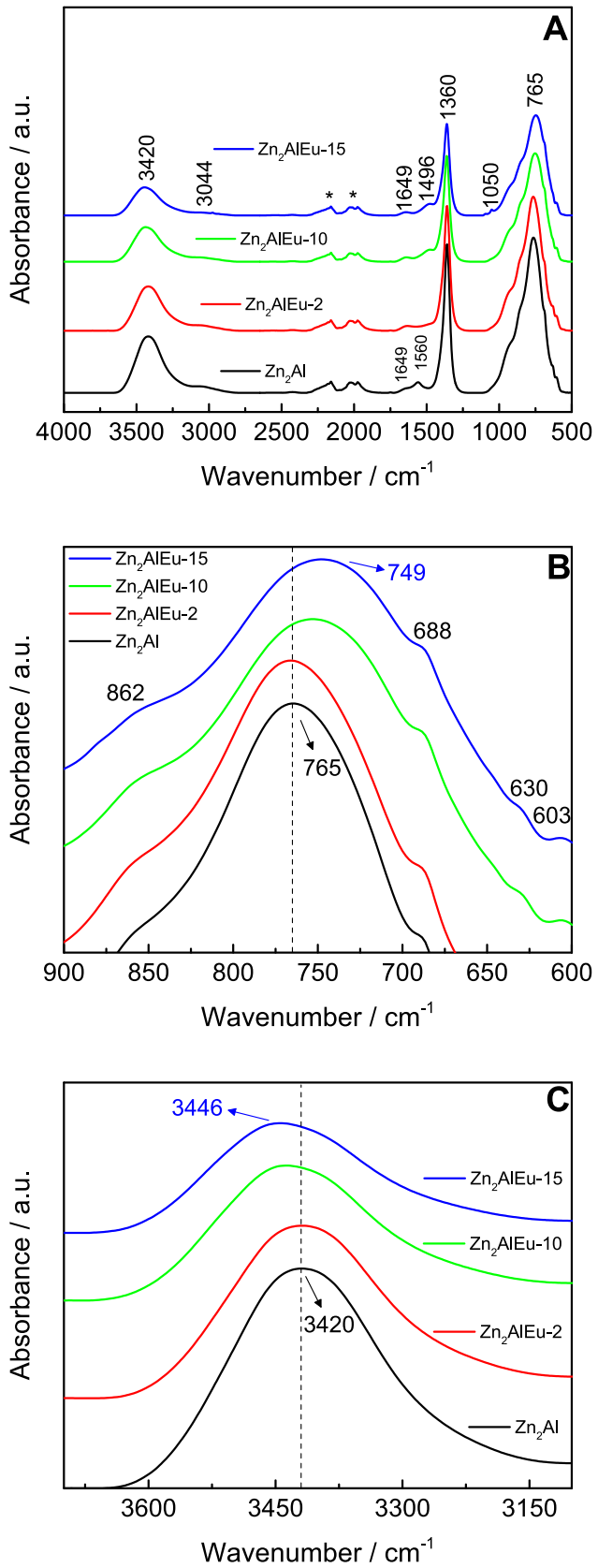

Fig. 2. (A) ATR-FT-IR spectra for the synthesized LDHs and enlargements for: (B) 900–600 $^{-1}$ region and (C) 3700–3100 cm^{-1} region. Asterisks (*) correspond to the diamond signals from the ATR equipment.

samples. The first one is characteristic of the symmetric stretching vibration of the carbonate anion (ν_1 mode) and keeps invariable in terms of wavenumber when the LDH is doped with Eu^{3+}. However, the rest of the bands undergo a decrease in energy (2–4 cm^{-1}) when Al^{3+} is substituted by Eu^{3+} in the brucite-like layers. The band at the lowest frequency is assigned to the deformation vibrations of the O–M−O bonds, and the remaining two bands are due to the OH^- units essentially linked to the Al^{3+} cation in the layers, also being influenced likely by the Zn^{2+} cation [44,45]. This supports the SXRD data that the average length of the M−O bonds in the LDH framework are modified by the Eu doping. Furthermore, this doping leads to the occurrence of other especially broad bands caused by the fluorescence of the lanthanide cation. In summary, from the SXRD, ATR-FT-IR and Raman data, it is evident that Zn_2Al-LDH framework is able to accommodate Eu^{3+} cations.

XPS spectra of the prepared LDHs are depicted in Fig. 3. As previously reported, the Al 2p peak centered at ~ 74 eV should be assigned to the Al^{3+} octahedrally coordinated in the LDH lattice (Fig. 3a) [46,47]. The Zn 2p signals for Zn^{2+} were detected at ~ 1045 and ~ 1022 eV corresponding to Zn $2p_{3/2}$ and Zn $2p_{1/2}$ respectively; Fig. 3B) [46]. A broad signal is observed in the XPS O 1 s region (Fig. 3C), which can be deconvoluted in three peaks corresponding to M−O bond (529.6 eV), M−OH (531.2 eV) and CO_3^{2-}/H_2O (532.4 eV), Fig. S2. The slight shift towards higher binding energies with an increased Eu content in Al 2p, Zn 2p and O 1 s confirms that the LDH framework is affected by the Eu doping [48]. The XPS Eu 3d region (Fig. 3D) shows four peaks related to the Eu $3d_{5/2}$ and Eu $3d_{3/2}$ chemical states of Eu^{2+} (1124.8 eV, Eu $3d_{5/2}$) and Eu^{3+} (1134.6 eV, Eu $3d_{5/2}$) [49,50]. These signals reveal that the incorporation of the Eu into the LDH framework entails a partial reduction of the Eu^{3+} cation at the surface, coexisting Eu^{2+} and Eu^{3+} in the brucite-like layers, as previously reported for ZnAlEu LDHs and other europium compounds [48,51].

The thermogravimetric curves for the samples are depicted in Fig. S3, are all representative of LDH compounds [52,53]. From room temperature to ~ 150 °C, there is a weight loss associated to surface water, which is weakly adsorbed onto the LDH particles. Then, there is a second weight loss from 150 up to ~ 290 °C due to the removal of interlayer water molecules which are stronger bonded to the layers and carbonates by means of hydrogen bonding. From 290 up to ~ 700 °C the decomposition of the carbonates together with the dehydroxylation of the layers takes place, the LDH structure being destroyed. No significant changes were found in the profiles of the samples. Using these data together those from XRF measurements, the LDH composition was calculated assuming that carbonate anions balanced the positive charge of the metal hydroxide layers (Table 2). The amount of europium in LDH was found to be approximately 20% lower than that used in the precursor solutions. This is usual in the preparation of lanthanide-containing LDHs, because the high ionic radius of the lanthanide cations makes more difficult their complete insertion into the LDH layers [37].

3.2. *Morphology and textural properties*

The SEM images of the samples are shown in Fig. S4. The undoped LDH crystals appear as platelets of hexagonal shape with rounded corners (*ca.* 100 × 80 nm), a typical morphology for LDHs synthesized by the coprecipitation method without posterior hydrothermal ageing [12,54]. When Eu doping was performed, imperfections are observed in the hexagonal platelets, because the growth of the crystalline domains is restricted by the distortions induced for the incorporation of a large cation like Eu^{3+}, as inferred from SXRD (Fig. 1). This feature was more observable for those LDHs having high Eu content (Zn_2AlEu-10 and Zn_2AlEu-15, Fig. S3C and S3D). In addition, EDX elemental mapping pointed to a uniform distribution of all elements forming the particles (Fig. S5). From the HRTEM images (Fig. S6), along with the variation in the shape, a thickening of the platelets is noticed at higher Eu content

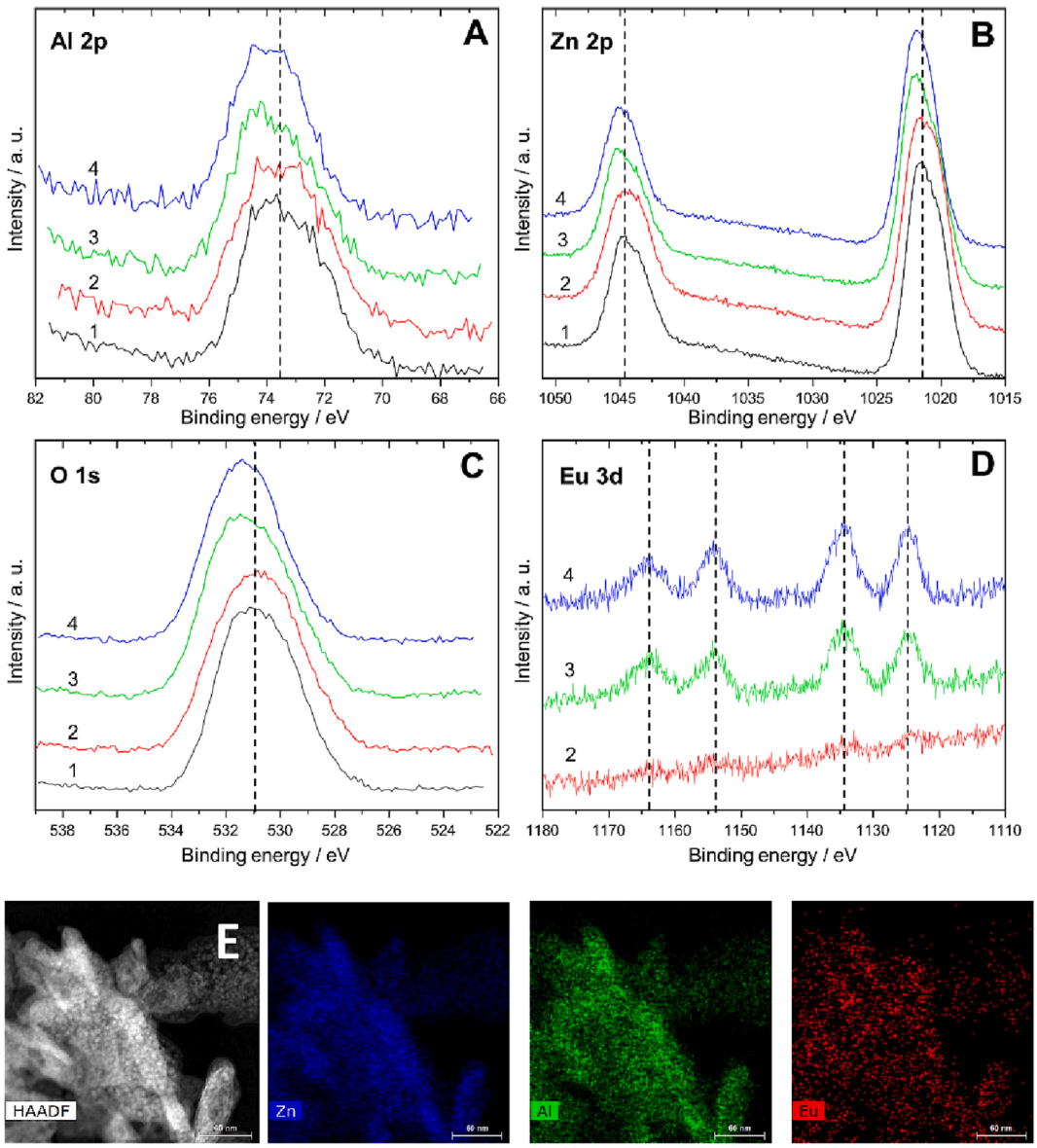

Fig. 3. XPS spectra of (A) Al 2p, (B) Zn 2p, (C) O 1 s and (D) Eu 3d for the samples Zn_2Al (1), Zn_2AlEu-2 (2), Zn_2AlEu-10 (3) and Zn_2AlEu-15 (4). (E) HAADF image of the Zn_2AlEu-15 sample and the corresponding EDX map (Zn: blue; Al: green; Eu: red).

Table 2
Compositional features for the synthesized LDHs.

Sample	Theoretical Zn:(Al + Eu) ratio	Experimental Zn:(Al + Eu) ratio	Theoretical Eu:(Al + Eu) ratio	Experimental Eu:(Al + Eu) ratio	Formula
Zn_2Al	2	2.06	0	0	$[Zn_{0.75}\ Al_{0.36}\ (OH)_{2.23}]\ (CO_3)_{0.18} \cdot 1.15\ H_2O$
Zn_2AlEu-2	2	2.02	0.02	0.0160	$[Zn_{0.75}\ Al_{0.36}\ Eu_{0.01}\ (OH)_{2.24}]\ (CO_3)_{0.19} \cdot 1.20\ H_2O$
Zn_2AlEu-10	2	2.05	0.10	0.0788	$[Zn_{0.75}\ Al_{0.34}\ Eu_{0.03}\ (OH)_{2.24}]\ (CO_3)_{0.18} \cdot 1.11\ H_2O$
Zn_2AlEu-15	2	2.08	0.15	0.1164	$[Zn_{0.75}\ Al_{0.32}\ Eu_{0.04}\ (OH)_{2.22}]\ (CO_3)_{0.18} \cdot 1.09\ H_2O$

samples (from ~13 nm in Zn_2Al to ~20 nm in Zn_2AlEu-15), indicating that structural changes provoked by the Eu insertion promote the layer stacking. Furthermore, the high-angle annular dark-field (HAADF) image and the corresponding elemental mapping were done for the Zn_2AlEu-15, verifying the homogenous element distribution and the successfully Eu doping (Fig. 3E).

Results from nitrogen adsorption–desorption isotherms for the samples are depicted in Fig. S7. Considering the IUPAC classification, these LDHs displayed a type II isotherm (H3 type hysteresis loop) which corresponds to materials with aggregates of plate-like particle morphology with slit-shaped pores. Although the Eu^{3+} doping did not modify the isotherm type, the BET specific surface area of the LDHs

underwent an increase with the Eu^{3+} doping, especially for the sample having the highest Eu content (Zn_2AlEu-15; Table 3). As denoted by SXRD and SEM results, the doped samples are poorest crystallized having influence in the aggregation of the platelets particles and, therefore, in the active surface area. Similarly, an upward trend could be seen in the pore volume values of the LDHs with increasing the doping level, probably promoted by the lower particle aggregation in the doped samples.

3.3. Optical and electronic properties

The UV–Vis spectra of the prepared LDHs are shown in Fig. 4A. The undoped sample, Zn_2Al LDH, exhibits a spectrum with an intense UV absorption tail, similar to that reported for carbonate-intercalated Zn_2Al LDHs [55–57]. This absorption might probably arise from the charge transfer phenomena in the LDH structure [58,59]. After Eu^{3+} doping, two broad bands appeared around 237 and 352 nm, which were ascribed to the oxygen-to-europium(III) ligand-to-metal charge transfer (LMCT) [60,61]. Furthermore, low-intensity absorption peaks were identified at 395, 465, 534 nm due to the $^7F_0 \rightarrow {}^5L_6$, $^7F_0 \rightarrow {}^5D_2$ and $^7F_0 \rightarrow {}^5D_1$ transitions from Eu^{3+} [62], respectively (Fig. 4A, inset), conferring to these photocatalysts a potential visible light activity. The band gap energy values of the samples were calculated by plotting the transformed Kubelka-Munk function versus the incident energy, Fig. S8. The band gap value of the undoped LDH was in agreement with that of Zn_2Al LDHs [12,63], whereas a red-shift about 0.1–0.3 eV was observed for Zn_2AlEu samples (Table 3).

VB-XPS was utilized to calculate the Valence Band Maximum (VBM) of the prepared LDHs, Fig. S9. This information, along with the band gap values, served to stablish the complete energy band scheme of the LDHs (Fig. 4B and Table 3). As shown in Fig. 4B, the Eu doping had more influence on the Conduction Band Maximum (CBM), increasing this potential with the doping amount. Thus, the CBM of the Zn_2AlEu-15 sample increased 0.22 eV respect to that of the raw LDH. The CBM potential exhibited the necessary energy to produce superoxide radicals ($E(O_2/\cdot O_2^-) = -0.33$ eV). Also, the formation of hydroxyl radicals should be thermodynamically feasible, as holes located in Valence Band Minimum (VBM) had higher reduction potential than that of the $H_2O/\cdot OH$ redox couple ($(E(H_2O/\cdot OH) = 2.34$ eV) [64]. Additionally, UPS measurements allowed to locate the Fermi Level for the studied LDHs (Fig. S10A). The Fermi Level was closer to the corresponding Valence Band Maximum for all samples, indicating their p-type role (Fig. S10B), similarly to other Zn_2Al LDHs [65,66]. Conversely, other Zn_xAl LDHs have been reported to show a n-type semiconductivity [67–69]. These differences are associated to the different M(II)/M(III) ratio and interlayer anion, factors that affect the electronic structure in LDH systems, as previously reported [66].

Table 3
Textural and electronic parameters of the synthesized LDHs.

Sample	Specific surface area[a] / m^2g^{-1}	Pore volume[b] / cm^3g^{-1}	Band gap[c] / eV	Valence Band Maximum[d] vs NHE / eV	Conduction Band Minimum[e] vs NHE / eV
Zn_2Al	54	0.12	3.51	2.83	− 0.68
Zn_2AlEu-2	55	0.13	3.39	2.74	− 0.65
Zn_2AlEu-10	57	0.15	3.33	2.71	− 0.62
Zn_2AlEu-15	74	0.20	3.22	2.76	− 0.46

Calculations by *a*: BET equation; *b*: single pore volume at $P/P_0 = 0.99$; *c*: Kubelka-Munk plots; *d*: VB-XPS; *e*: Valence Band Maximun – band gap value.

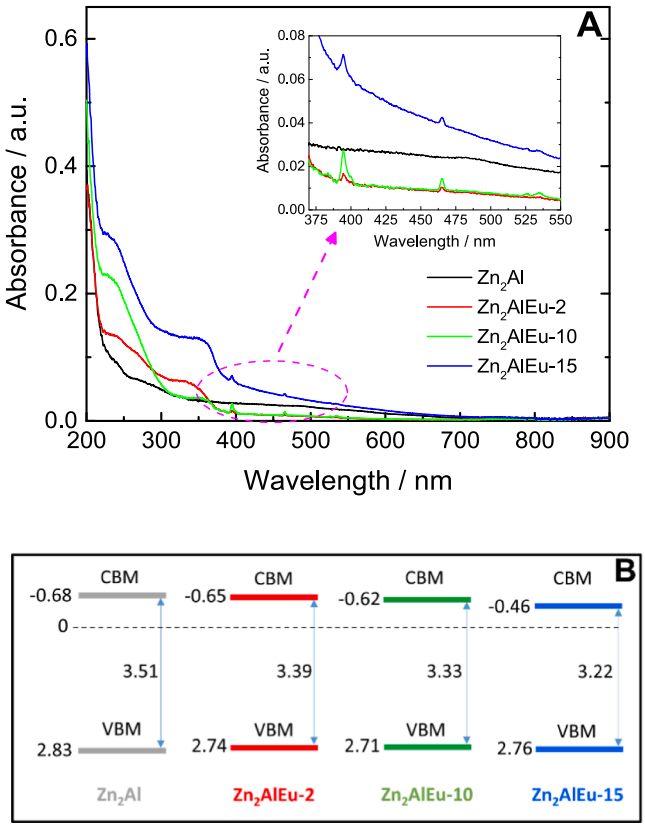

Fig. 4. (A) UV–Vis absorption spectra and (B) schematic band diagrams for the synthesized LDHs (values in eV vs NHE).

3.4. Photocatalytic De-NO_x performance

The photocatalytic efficiency of the samples was evaluated by considering their capacity to remove a continuous nitrogen oxide gas flow in a photocatalytic reactor under different illumination sources. Fig. 5A and 5B show the monitored NO concentration profiles obtained for the synthesized LDHs subjected to photocatalytic experiments under UV–Vis and visible light, respectively. All LDHs were photocatalytically functional, removing part of the NO pollutant when they were light irradiated. As our group reported in previous works [10,15,17,70], once the LDH photocatalyst is light irradiated, the electrons (e^-) and holes (h^+) reaching the photocatalysts surface are able to produce radical ROS species ($\cdot OH$, $\cdot O_2^-$) by interaction with the water and oxygen molecules from the environment. Consequently, the strong oxidant ROS species promote the following sequential oxidation of NO gas molecules: $NO \rightarrow NO_2^- \rightarrow NO_2 \rightarrow NO_3^-$ [71], which in term are removed from the atmosphere as nitrite/nitrates species deposited onto the photocatalyst [71,72]. Interestingly, E_{NO} was clearly enhanced for europium containing samples although a linear trend with the Eu doping level was not observed: Zn_2Al (33.2 %) < Zn_2AlEu-10 (49.8 %) < Zn_2AlEu-2 (55.1 %) < Zn_2AlEu-15 (58.6 %), Fig. 5C. The evolution observed for the E_{NO} index does not seem to be influenced by the specific surface area values of the samples since these values are similar to each other and, therefore, the observed photocatalytic results might be related to differences in the electronic properties, as will be commented on later. When the De-NO_x tests were performed under visible light irradiation, even though the NO removal efficiency of the samples was lower compared to that obtained under UV–Vis light, it was observed that the presence of Eu in the LDH framework was the key factor to boost the photocatalytic activity, Fig. 5B. By comparing both E_{NO} values, those obtained under UV–Vis or visible light (Fig. 5C), it is concluded that Zn_2AlEu-15 sample works mainly by visible light activation. In fact, its high NO removal efficiency

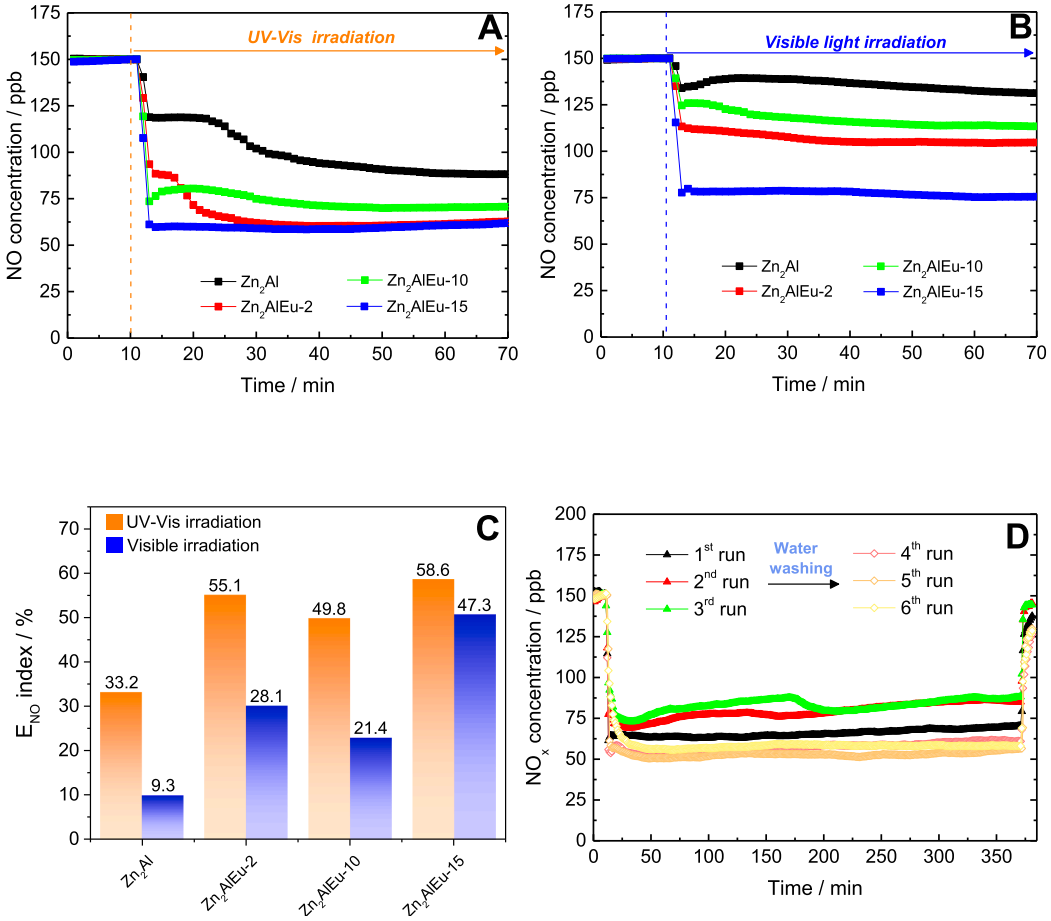

Fig. 5. NO gas concentration profiles during the photocatalytic tests under (A) UV–Vis light and (B) visible light illumination. (C) NO removal efficiency of the studied photocatalysts. (D) Successive long irradiation De-NO_x tests for Zn_2AlEu-15 LDH under UV–Vis light illumination.

value (E_{NO} = 47 %) measured under visible light clearly surpasses to those previously reported for doped LDHs in De-NO_x photocatalysis (Table S1), which highlights the role of Eu as doping element for LDH photocatalysts. Although the samples were able to remove the NO pollutant, it is mandatory to check the evolution of the NO_2 gas, an intermediate species which may be generated during the De-NO_x process. This gas is much more hazardous than the NO gas and, therefore, its release to the atmosphere must be avoided considering an environmental application for these photocatalysts [73]. It was verified that the NO_2 production was negligible for the studied LDHs, lower than 8 ppb (Fig. S11A, B), indicating an efficient photooxidation of the NO gas towards nitrates and nitrites species. Indeed, the Selectivity parameter was calculated, which refers to the capacity of the photocatalyst to completely oxidize the NO gas (Fig. S11C). As expected for LDH De-NO_x photocatalysts [10–13], the Zn_2Al and Zn_2AlEu LDHs maintained outstanding selectivity values, $S > 90$ % (Fig. S11C).

Moreover, consecutive De-NO_x tests were performed over the Zn_2AlEu-15 LDH to evaluate its NO_x removal efficiency in a long-term pollution scenario (Fig. 5D). Zn_2AlEu-15 kept a E_{NOx} value around 50 % during 3 long irradiation tests (total irradiated time = 18 h), which indicates an outstanding cyclability capacity compared to the recent reported De-NO_x photocatalysts, considering the extended irradiation period [74–79]. An expected low decrease of the NO_x removal activity was observed after the described tests. This is a consequence of the formation of the products coming from the sequential photochemical oxidation of NO gas molecules, which end up deposited as nitrates/nitrites products on the surface of the photocatalyst, as confirmed by in-situ DRIFTS experiments, Fig. S12 [13,72]. However, the highly soluble nitrates/nitrites products are easily removed by a simple water washing of the sample (stirring 1 h with 80 mL water). This has been enough to recover the photocatalytic efficiency, the active sites of the photocatalyst being again available to perform a new De-NO_x test. In fact a slight improved NO removal efficiency (+8%) was observed (Fig. 5D, 4th run), in line with similar observation for other reused LDH De-NO_x photocatalysts [11]. Since the preservation of the LDH structure after the photocatalytic and washing processes was evidenced by XRD and ATR-FT-IR measurements (Fig. S13), the improved NO_x removal efficiency of the washed sample should be associated to a better particle dispersion, which for LDHs is known to be affected by the water washing and drying steps [80].

3.5. *Insights into the doping effect and the De-NO_x mechanism*

Steady-state Photoluminescence (PL) measurements of the LDHs were carried out in order to shed some insights into the role of Eu. Fig. 6A depicts the PL emission spectra of the prepared LDHs. Broad bands below 500 nm were observed for all samples, which are assigned to the characteristic PL signals of the Zn_2Al structure [11,81]. Also, new narrow bands were noticeable above 500 nm when the Eu cation was introduced into the LDH structure, these signals being typically attributed to the Eu^{3+} *f-f* transitions. In this regard, noteworthy information about the Eu^{3+} environment can be obtained by studying the relative intensities of theses transitions in the PL emission spectra. According to the Judd – Ofelt theory, whereas the $^5D_0 \rightarrow {}^7F_1$ transition (magnetic-dipole transition) is not sensitive to the Eu chemical environment, the intensity of the $^5D_0 \rightarrow {}^7F_2$ electric dipole transition is highly dependent on the local geometry of the Eu^{3+}. For a perfectly centrosymmetric environment, very low radiative transition rates should be expected for

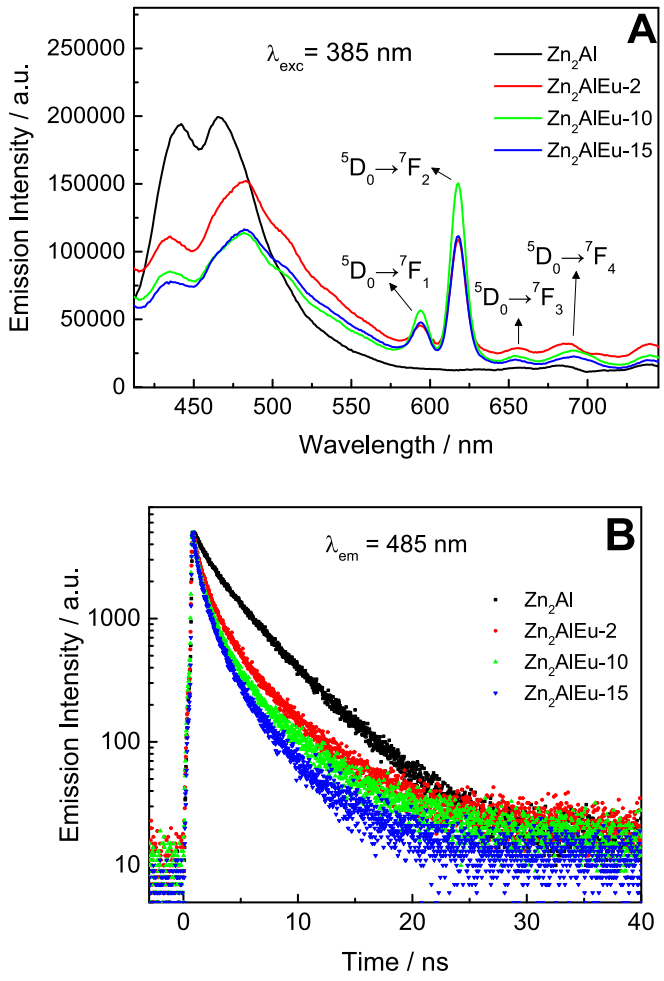

Fig. 6. (A) Steady-state PL and (B) Time-resolved PL spectra for the studied LDHs.

the $^5D_0 \rightarrow {}^7F_2$ emissions [82,83]. However, this emission is the most intense for the Zn_2AlEu LDHs (Fig. 6A), which clearly rules out the characteristic octahedral symmetry for the metal sites in LDHs. This result agrees with others studies on Eu-containing LDHs and demonstrate that the high ionic radius of Eu^{3+} induces changes in the coordination environment and, therefore, leads to a disordered lattice and/or structural defects a [33,82–84]. Regarding the Eu^{2+} cation, the most intense emission transitions ($^5D \rightarrow {}^4F$) could not be investigated as they appear around 390 nm, being hidden by the PL emission of the LDH matrix [85].

Additional information about the local symmetry around the Eu^{3+} centers in the LDH structure can be obtained from the Judd-Ofelt intensity parameters ($\Omega_{2,4}$; Table 4). Whereas the Ω_2 informs about angular changes in the coordination of the lanthanide cation, the Ω_4 is influenced by the polarizability of the first shell of the atoms bonded to the Eu^{3+} [86]. Looking at Table 4, it is noted that the Ω_2 *and* Ω_4 parameters for Zn_2AlEu-2 are the highest among the studied samples, indicating that the Eu^{3+} center has a somewhat different coordination on this sample. This would explain the relatively high NO_x removal efficiency observed for this sample unlike its low doping level, as deviations from the typical octahedral coordination in LDHs should create strains/defects that influence the photocharges movement [3,4]. As an additional data, the expectable Eu^{3+} absorptions bands were detected when measuring the excitation spectra of the doped samples (Fig. S14) [87,88].

Table 4
Judd-Ofelt intensity parameters for the transitions $^5D_0 \rightarrow {}^7F_2$ and $^5D_0 \rightarrow {}^7F_4$ ($\Omega_{2,4}$) and photoluminescence parameters obtained for the synthesized LDHs.

	Ω_2 / 10^{-20} cm^2	Ω_4 / 10^{-20} cm^2	τ_1 / ns	τ_2 / ns	Quantum yield / %
Zn_2Al	–	–	1.39	4.62	12.0
Zn_2AlEu-2	12.0	3.0	0.95	4.72	8.9
Zn_2AlEu-10	7.9	2.2	0.78	4.41	4.7
Zn_2AlEu-15	8.1	2.4	0.66	3.54	2.2

On the other hand, the intensity of the PL emission signal related to the Zn_2Al LDH showed a significant decrease when the Eu doping was carried out (Fig. 6A). Additional information was obtained by measuring the TRPL decays (Fig. 6B). The curves were fitted to a bi-exponential function, the lifetimes being showed in Table 4. Both τ_1 and τ_2 decays followed the same trend: Zn_2AlEu-15 < Zn_2AlEu-10 < Zn_2AlEu-2 < Zn_2Al, which indicates an increasing quenching of the PL of the Zn_2Al LDH at higher concentrations of the Eu^{3+} cations. The PL quenching was confirmed by measuring the absolute PL quantum yield (PLQY), where an almost 6-fold decrease of the PLQY was detected when comparing the raw undoped Zn_2Al LDH with the sample containing the highest amount of Eu (Table 4). The observed PL quenching is associated to a novel deactivation pathway of the excited state of the LDH compound. The effect of Eu doping on the energetic scheme of ZnAl-LDH compounds has been recently reported, showing the formation of electronic energy levels associated with the 4f orbitals within the bandgap of the LDH matrix [48]. This energetic configuration was proved to be consistent with an enhanced energy transfer rate of excited electrons from the LDH CBM to the Eu^{3+} 4f energy levels. Thus, the PL quenching observed in the measurements is then ascribed to the mentioned energy transfer process which may be beneficial for the photocatalytic process [48]. Indeed, the longer lifetime of the electrons in the Eu-related energy states would facilitate the formation of larger amount of ROS species (by interaction with the oxygen and water molecules) in the Eu doped samples contributing to an enhancement of the De-NO_x photoactivity.

In this sense, to explore the ability of the samples to produce ROS radicals, EPR spin-trapping experiments were performed under light irradiation. As shown in Fig. 7, the typical signals corresponding to trapped hydroxyl radical (DMPO–·OH adduct; 1:2:2:1 peak intensity ratio; Fig. 7A) and superoxide radical (DMPO–·O_2^-; 1:1:1:1 peak intensity ratio; Fig. 7B) were observed [89]. By comparison, the signals corresponding to hydroxyl radical are well defined and more intense to those of superoxide radical, suggesting that ·OH radicals are dominant in the photocatalytic process. In addition, the DMPO–·OH adduct signal for Zn_2AlEu-15 showed a higher intensity compared to the undoped LDH. The higher availability of ·OH radicals should be in line with a decrease of the e^-/h^+ recombination, as predicted from PL studies (Fig. 6a) and agrees with the obtained photocatalytic De-NO_x tests, highlighting the enhancement of the hydroxyl radicals generation by the doped samples.

4. Conclusions

Zn_2Al-CO_3 LDHs with increasing levels of doping Eu^{3+} (Zn_2AlEu_x; x = 0.01–0.04) have been prepared and studied as photocatalysts for oxidation of NO_x gases. The analytical data indicate that all LDHs were phase pure. The Eu^{3+} cation, is larger than Al^{3+} and so when introduced into the LDH lattice, causes modifications to M−O interactions. Moreover, the Eu^{3+} doping induces an enhancement in the light absorption of the LDHs and their band gap values were decreased by ~ 0.3 eV. The Zn_2AlEu_x LDHs exhibited outstanding selectivity and higher NO_x removal efficiencies under UV–Vis and specially under visible light (420 nm). The optimal doped LDH (Zn_2AlEu-15) yielded a 5-fold increase of the photocatalytic efficiency when compared to the original Zn_2Al LDH. This enhanced photocatalytic improvement was ascribed to promoted charge separation (probably from the LDH to the *f* levels of Eu^{3+}) and to a higher production of ·OH radicals by the doped LDHs. As a result, we

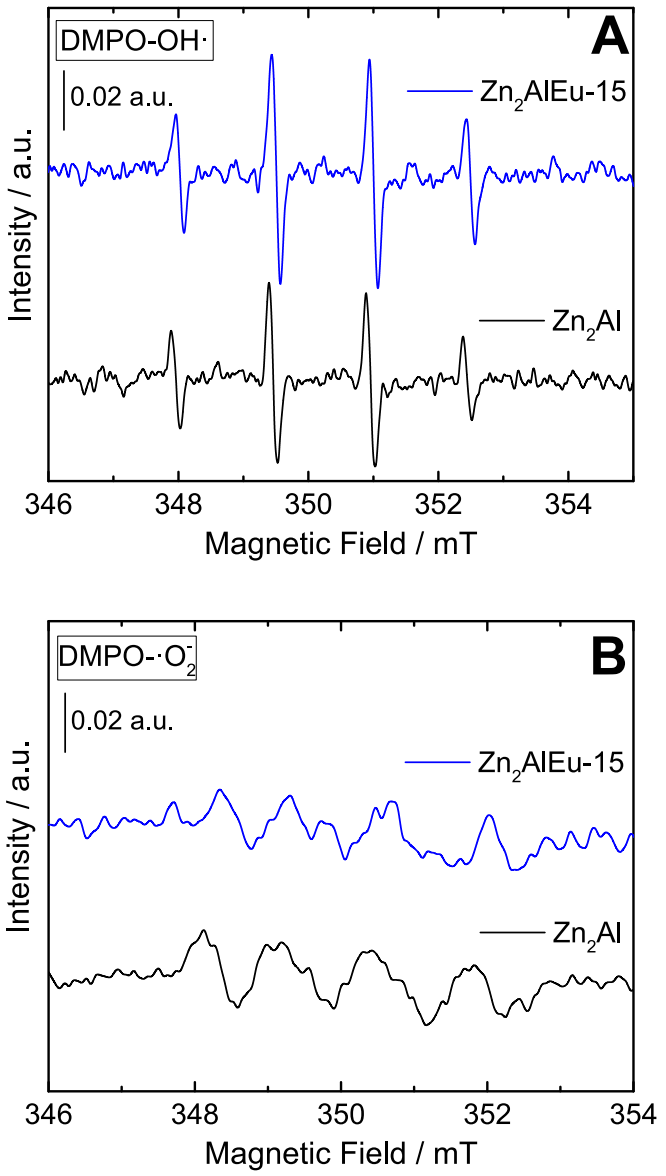

Fig. 7. DMPO spin-trapping EPR spectra for the Zn_2Al, Zn_2AlEu-2 and Zn_2AlEu-15 LDHs: (A) DMPO-·OH and (B) DMPO-·O_2^- adducts.

consider Eu-doped LDHs to be promising candidates for the NO_x photooxidation and also for other related photocatalytic applications.

Declaration of Competing Interest

The authors declare that they have no known competing financial interests or personal relationships that could have appeared to influence the work reported in this paper.

Data availability

Data will be made available on request.

Acknowledgements

This work was supported by the Junta de Andalucía, Spain (PAI Groups FQM-214 and FQM-175, FQM-192) Agencia Estatal de Investigación and Spanish Government (PID2020-117516 GB-I00, PID2020-117832RB-100). Chunping Chen acknowledges support from SCG Chemicals ublic Co Ltd. The authors acknowledge the Diamond Light Source for powder diffraction measurements. Adrián Pastor is grateful for a contract received by Universidad de Córdoba (Plan Propio de Investigación de la Universidad de Córdoba 2022) and for funding from Ministerio de Universidades (FPU2016-05041; EST19/00179). Funding for open access charge: Universidad de Córdoba / CBUA.

Appendix A. Supplementary data Details about characterization techniques, Raman spectra, XPS, TGA, SEM images, EDX, HRTEM images, nitrogen adsorption-desorption isotherms, Kubelka-Munk transformed function plots, VB-XPS spectra, UPS spectra, energy band diagrams, NO_2 concentration profiles, successive long irradiation De-NO_x tests, in situ DRIFTS spectra characterization after De-NO_x photocatalytic tests and excitation spectra.

Supplementary data to this article can be found online at https://doi.org/10.1016/j.cej.2023.144464.

References

[1] V. Rives, Layered Double Hydroxides: Present and Future, Nova Science Publishers Inc, New York, 2001.
[2] F. Cavani, F. Trifirò, A. Vaccari, Hydrotalcite-type anionic clays: Preparation, properties and applications, Catal. Today 11 (1991) 173–301, https://doi.org/10.1016/0920-5861(91)80068-K.
[3] X. Bian, S. Zhang, Y. Zhao, R. Shi, T. Zhang, Layered double hydroxide-based photocatalytic materials toward renewable solar fuels production, InfoMat. 3 (2021) 719–738, https://doi.org/10.1002/inf2.12192.
[4] S.-F. Ng, M.Y.L. Lau, W.-J. Ong, Engineering Layered Double Hydroxide-Based Photocatalysts Toward Artificial Photosynthesis: State-of-the-Art Progress and Prospects, Sol. RRL. 5 (2021) 2000535, https://doi.org/10.1002/SOLR.202000535.
[5] Z.-Z. Yang, J.-J. Wei, G.-M. Zeng, H.-Q. Zhang, X.-F. Tan, C. Ma, X.-C. Li, Z.-H. Li, C. Zhang, A review on strategies to LDH-based materials to improve adsorption capacity and photoreduction efficiency for CO_2, Coord. Chem. Rev. 386 (2019) 154–182.
[6] K.H. Kim, S. Kim, B.C. Moon, J.W. Choi, H.M. Jeong, Y. Kwon, S. Kwon, H.S. Choi, J.K. Kang, Quadruple metal-based layered structure as the photocatalyst for conversion of carbon dioxide into a value added carbon monoxide with high selectivity and efficiency, J. Mater. Chem. A 5 (2017) 8274–8279, https://doi.org/10.1039/c7ta01623a.
[7] H. Boumeriame, E.S. Da Silva, A.S. Cherevan, T. Chafik, J.L. Faria, D. Eder, Layered double hydroxide (LDH)-based materials: A mini-review on strategies to improve the performance for photocatalytic water splitting, J. Energy Chem. 64 (2021) 406–431, https://doi.org/10.1016/j.jechem.2021.04.050.
[8] P. Miao, J. Zhao, R. Shi, Z. Li, Y. Zhao, C. Zhou, T. Zhang, Layered double hydroxide engineering for the photocatalytic conversion of inactive carbon and nitrogen molecules, ACS ES&T Eng. 2 (2022) 1088–1102, https://doi.org/10.1021/acsestengg.1c00489.
[9] G. Zhang, X. Zhang, Y. Meng, G. Pan, Z. Ni, S. Xia, Layered double hydroxides-based photocatalysts and visible-light driven photodegradation of organic pollutants: a review, Chem. Eng. J. 392 (2020), 123684, https://doi.org/10.1016/j.cej.2019.123684.
[10] J. Fragoso, M.A. Oliva, L. Camacho, M. Cruz-Yusta, G. de Miguel, F. Martin, A. Pastor, I. Pavlovic, L. Sánchez, Insight into the role of copper in the promoted photocatalytic removal of NO using $Zn_{2-x}Cu_xCr$-CO_3 layered double hydroxide, Chemosphere 275 (2021) 130030.
[11] A. Pastor, F. Rodriguez-Rivas, G. de Miguel, M. Cruz-Yusta, F. Martin, I. Pavlovic, L. Sánchez, Effects of Fe^{3+} substitution on Zn-Al layered double hydroxides for enhanced NO photochemical abatement, Chem. Eng. J. 387 (2020), 124110, https://doi.org/10.1016/j.cej.2020.124110.
[12] F. Rodriguez-Rivas, A. Pastor, C. Barriga, M. Cruz-Yusta, L. Sánchez, I. Pavlovic, Zn-Al layered double hydroxides as efficient photocatalysts for NOx abatement, Chem. Eng. J. 346 (2018) 151–158, https://doi.org/10.1016/j.cej.2018.04.022.
[13] X. Lv, J. Zhang, X. Dong, J. Pan, W. Zhang, W. Wang, G. Jiang, F. Dong, Layered double hydroxide nanosheets as efficient photocatalysts for NO removal: band structure engineering and surface hydroxyl ions activation, Appl. Catal. B Environ. 277 (2020), 119200, https://doi.org/10.1016/j.apcatb.2020.119200.
[14] W. Huo, T. Cao, X. Liu, W. Xu, B. Dong, Y. Zhang, F. Dong, Anion intercalated layered-double-hydroxide structure for efficient photocatalytic NO remove, Green Energy Environ. 4 (2019) 270–277, https://doi.org/10.1016/j.gee.2018.11.001.
[15] A. Pastor, C. Chen, G. de Miguel, F. Martin, M. Cruz-Yusta, J.-C. Buffet, D. O'Hare, I. Pavlovic, L. Sánchez, Aqueous miscible organic solvent treated NiTi layered double hydroxide De-NOx photocatalysts, Chem. Eng. J. 429 (2022) 132361.
[16] F. Rodriguez-Rivas, A. Pastor, G. de Miguel, M. Cruz-Yusta, I. Pavlovic, L. Sánchez, Cr^{3+} substituted Zn-Al layered double hydroxides as UV–Vis light photocatalysts for NO gas removal from the urban environment, Sci. Total Environ. 706 (2020), 136009, https://doi.org/10.1016/j.scitotenv.2019.136009.
[17] J. Fragoso, A. Pastor, M. Cruz-Yusta, F. Martin, G. de Miguel, I. Pavlovic, M. Sánchez, L. Sánchez, Graphene quantum dots/NiTi layered double hydroxide

heterojunction as a highly efficient De-NOx photocatalyst with long persistent post-illumination action, Appl. Catal. B Environ. 322 (2023), https://doi.org/10.1016/j.apcatb.2022.122115.
[18] Y. Miao, R. Guo, J. Gu, Y. Liu, G. Wu, C. Duan, W. Pan, Z-scheme Bi/$Bi_2O_2CO_3$/layered double-hydroxide nanosheet heterojunctions for photocatalytic CO_2 reduction under visible light, ACS Appl. Nano Mater. 4 (2021) 4902–4911, https://doi.org/10.1021/acsanm.1c00458.
[19] S. Jatav, M. Herber, H. Xiang, E.H. Hill, Layered double hydroxide-bismuth molybdate hybrids toward water remediation via selective adsorption of anionic species, ACS Appl. Mater. Interfaces 14 (2022) 51921–51930, https://doi.org/10.1021/acsami.2c14979.
[20] H. Wang, Y. Xia, X. Wang, Y. Han, X. Jiao, D. Chen, Interfacial coupling effect on electron transport in hierarchical TaON/Au/ZnCo-LDH photoanode with enhanced photoelectrochemical water oxidation, ACS Appl. Mater. Interfaces 11 (2019) 33062–33073, https://doi.org/10.1021/acsami.9b11521.
[21] R.-T. Guo, Z.-x. Bi, Z.-D. Lin, X. Hu, J. Wang, X. Chen, W.-G. Pan, Carbon quantum dots-modified Z-scheme $Bi_{12}O_{17}Cl_2$/NiAl-LDH for significantly boosting photocatalytic CO_2 reduction, J. Colloid Interface Sci. 627 (2022) 343–354.
[22] J.L. Xochihua Juan, C. Solis Maldonado, R.A. Luna Sánchez, O.J. Enciso Díaz, M. R. Rojas Ronquillo, L. Sandoval-Rangel, N. Pineda Aguilar, N.A. Ramos Delgado, D. X. Martínez-Vargas, TiO_2 doped with europium (Eu): synthesis, characterization and catalytic performance on pesticide degradation under solar irradiation, Catal. Today 394–396 (2022) 304–313, https://doi.org/10.1016/j.cattod.2021.08.024.
[23] E. Cerrato, E. Gaggero, P. Calza, M.C. Paganini, The role of cerium, europium and erbium doped TiO_2 photocatalysts in water treatment: a mini-review, Chem. Eng. J. Adv. 10 (2022), 100268, https://doi.org/10.1016/J.CEJA.2022.100268.
[24] A.R. Khataee, A. Karimi, R.D.C. Soltani, M. Safarpour, Y. Hanifehpour, S.W. Joo, Europium-doped ZnO as a visible light responsive nanocatalyst: Sonochemical synthesis, characterization and response surface modeling of photocatalytic process, Appl. Catal. A 488 (2014) 160–170, https://doi.org/10.1016/J.APCATA.2014.09.039.
[25] J.C. Sin, S.M. Lam, Hydrothermal synthesis of europium-doped flower-like ZnO hierarchical structures with enhanced sunlight photocatalytic degradation of phenol, Mater. Lett. 182 (2016) 223–226, https://doi.org/10.1016/J.MATLET.2016.06.126.
[26] J.C. Sin, S.M. Lam, I. Satoshi, K.T. Lee, A.R. Mohamed, Sunlight photocatalytic activity enhancement and mechanism of novel europium-doped ZnO hierarchical micro/nanospheres for degradation of phenol, Appl. Catal. B Environ. 148–149 (2014) 258–268, https://doi.org/10.1016/J.APCATB.2013.11.001.
[27] S. Yao, C. Sui, Z. Shi, Preparation and characterization of visible-light-driven europium doped mesoporous titania photocatalyst, J. Rare Earths 29 (2011) 929–933, https://doi.org/10.1016/S1002-0721(10)60571-6.
[28] L. Diamandescu, F. Vasiliu, D. Tarabasanu-Mihaila, M. Feder, A.M. Vlaicu, C. M. Teodorescu, D. Macovei, I. Enculescu, V. Parvulescu, E. Vasile, Structural and photocatalytic properties of iron- and europium-doped TiO_2 nanoparticles obtained under hydrothermal conditions, Mater. Chem. Phys. 112 (2008) 146–153, https://doi.org/10.1016/J.MATCHEMPHYS.2008.05.023.
[29] Y. Zhang, H. Zhang, Y. Xu, Y. Wang, Europium doped nanocrystalline titanium dioxide: preparation, phase transformation and photocatalytic properties, J. Mater. Chem. 13 (2003) 2261–2265, https://doi.org/10.1039/B305538H.
[30] A. Zhang, J. Zhang, Effects of europium doping on the photocatalytic behavior of BiVO4, J. Hazard. Mater. 173 (2010) 265–272, https://doi.org/10.1016/J.JHAZMAT.2009.08.079.
[31] Y. Tian, L. Zhang, J. Zhang, A superior visible light-driven photocatalyst: Europium-doped bismuth tungstate hierarchical microspheres, J. Alloy. Compd. 537 (2012) 24–28, https://doi.org/10.1016/J.JALLCOM.2012.05.029.
[32] H. Wu, J. Peng, H. Sun, Q. Ruan, H. Dong, Y. Jin, Z. Sun, Y. Hu, Surface activation of calcium tungstate by europium doping for improving photocatalytic performance: towards lanthanide site photocatalysis, Chem. Eng. J. 432 (2022), 134339, https://doi.org/10.1016/J.CEJ.2021.134339.
[33] X. Gao, M. Hu, L. Lei, D. O'Hare, C. Markland, Y. Sun, S. Faulkner, Enhanced luminescence of europium-doped layered double hydroxides intercalated by sensitiser anions, Chem. Commun. 47 (2011) 2104–2106, https://doi.org/10.1039/C0CC04123H.
[34] V.A. Drits, A.S. Bookin, Crystal Structure and X-ray Identification of Layered Double Hydroxides, in: V. Rives (Ed.), Layer. Double Hydroxides Present Futur., Nova Science Publishers Inc, New York, 2001: pp. 41–100.
[35] D.G. Evans, R.C.T. Slade, Structural aspects of Layered Double Hydroxides, in: X. Duan, D.G. Evans (Eds.), Layer. Double Hydroxides, Springer, Berlin, Heidelberg, Heidelberg, 2005: pp. 1–87. doi:https://doi.org/10.1007/430_005.
[36] Y. Zhao, J.-G. Li, F. Fang, N. Chu, H. Ma, X. Yang, Structure and luminescence behaviour of as-synthesized, calcined, and restored MgAlEu-LDH with high crystallinity, Dalt. Trans. 41 (2012) 12175, https://doi.org/10.1039/c2dt31249b.
[37] T. Posati, F. Costantino, L. Latterini, M. Nocchetti, M. Paolantoni, L. Tarpani, New insights on the incorporation of lanthanide ions into nanosized layered double hydroxides, Inorg. Chem. 51 (2012) 13229–13236, https://doi.org/10.1021/ic301584g.
[38] J.T. Kloprogge, R.L. Frost, Infrared and Raman Spectroscopic Studies of Layered Double Hydroxides (LDHs), in: V. Rives (Ed.), Layer. Double Hydroxides Present Futur., Nova Science Publishers Inc, New York, 2001: pp. 153–216.
[39] M.A. González, R. Trócoli, I. Pavlovic, C. Barriga, F. La Mantia, Capturing Cd(II) and Pb(II) from contaminated water sources by electro-deposition on hydrotalcite-like compounds, PCCP 18 (2016) 1838–1845, https://doi.org/10.1039/C5CP05235A.
[40] A.W. Musumeci, Z.P. Xu, S.V. Smith, R.F. Minchin, D.J. Martin, Layered double hydroxide nanoparticles incorporating terbium: applicability as a fluorescent probe and morphology modifier, J. Nanoparticle Res. 12 (2010) 111–120, https://doi.org/10.1007/s11051-008-9583-9.
[41] J.T. Kloprogge, R.L. Frost, Fourier Transform Infrared and Raman Spectroscopic Study of the Local Structure of Mg-, Ni-, and Co-Hydrotalcites, J. Solid State Chem. 146 (1999) 506–515, https://doi.org/10.1006/JSSC.1999.8413.
[42] E.M. Seftel, E. Popovici, M. Mertens, P. Cool, E.F. Vansant, Infrared and Raman spectroscopic study of Sn-containing Zn/Al-layered double hydroxides, J. Optoelectron. Adv. Mater. 10 (2008) 3477–3481.
[43] J.T. Kloprogge, L. Hickey, R.L. Frost, FT-Raman and FT-IR spectroscopic study of synthetic Mg/Zn/Al-hydrotalcites, J. Raman Spectrosc. 35 (2004) 967–974, https://doi.org/10.1002/jrs.1244.
[44] J. Pérez-Ramírez, G. Mul, J.A. Moulijn, In situ Fourier transform infrared and laser Raman spectroscopic study of the thermal decomposition of Co–Al and Ni–Al hydrotalcites, Vib. Spectrosc 27 (2001) 75–88, https://doi.org/10.1016/S0924-2031(01)00119-9.
[45] S. Paikaray, M.J. Hendry, The role of trivalent cations and interlayer anions on the formation of layered double hydroxides in an oxic-CO2 medium, Appl. Surf. Sci. 263 (2012) 633–639, https://doi.org/10.1016/J.APSUSC.2012.09.125.
[46] L. Wu, B. Peng, Q. Li, Q. Wang, X. Yan, K. Li, Q. Lin, Effects of Cu^{2+} incorporation on ZnAl-layered double hydroxide, New J. Chem. 44 (2020) 5293–5302, https://doi.org/10.1039/D0NJ00278J.
[47] M.M. Rao, B.R. Reddy, M. Jayalakshmi, V.S. Jaya, B. Sridhar, Hydrothermal synthesis of Mg–Al hydrotalcites by urea hydrolysis, Mater. Res. Bull. 40 (2005) 347–359, https://doi.org/10.1016/J.MATERRESBULL.2004.10.007.
[48] D.-K. Cho, S.-S. Lee, J.-S. Lim, S.-H. Baek, I.-K. Park, Visible light-emission from Eu-doped ZnAl layered-double hydroxide, Ceram. Int. 43 (2017) 9686–9690, https://doi.org/10.1016/j.ceramint.2017.04.142.
[49] R. Vercaemst, D. Poelman, L. Fiermans, R.L. Van Meirhaeghe, W.H. Laflère, F. Cardon, A detailed XPS study of the rare earth compounds EuS and EuF_3, J. Electron Spectros. Relat. Phenomena. 74 (1995) 45–56, https://doi.org/10.1016/0368-2048(95)02349-6.
[50] P. Rosenberger, M. Müller, Europium oxide: Growth guide for the first monolayers on oxidic substrates, Phys. Rev. Mater. 6 (2022), 044404, https://doi.org/10.1103/PhysRevMaterials.6.044404.
[51] V.G. Pol, R. Reisfeld, A. Gedanken, Sonochemical synthesis and optical properties of europium oxide nanolayer coated on titania, Chem. Mater. 14 (2002) 3920–3924, https://doi.org/10.1021/cm0203464.
[52] V. Rives, Study of Layered Double Hydroxides by Thermal Methods, in: V. Rives (Ed.), Layer. Double Hydroxides Present Futur., Nova Science Publishers Inc, New York, 2001: pp. 127–152.
[53] Y. Chen, S. Zhou, F. Li, Y. Chen, Synthesis and photoluminescence of Eu-doped Zn/Al layered double hydroxides, J. Mater. Sci. 45 (2010) 6417–6423, https://doi.org/10.1007/s10853-010-4725-8.
[54] S. Radhakrishnan, K. Lauwers, C.V. Chandran, J. Trébosc, S. Pulinthanathu Sree, J. A. Martens, F. Taulelle, C.E.A. Kirschhock, E. Breynaert, NMR Crystallography Reveals Carbonate Induced Al-Ordering in ZnAl Layered Double Hydroxide, Chem. - A Eur. J. 27 (2021) 15944–15953, https://doi.org/10.1002/chem.202101275.
[55] C.-W. Jeon, S.-S. Lee, I.-K. Park, Flexible Visible-Blind Ultraviolet Photodetectors Based on ZnAl-Layered Double Hydroxide Nanosheet Scroll, ACS Appl. Mater. Interfaces 11 (2019) 35138–35145, https://doi.org/10.1021/acsami.9b12082.
[56] S. Zhang, Y. Zhao, R. Shi, C. Zhou, G.I.N. Waterhouse, L.Z. Wu, C.H. Tung, T. Zhang, Efficient Photocatalytic Nitrogen Fixation over $Cu^{\delta+}$-Modified Defective ZnAl-Layered Double Hydroxide Nanosheets, Adv. Energy Mater. 10 (2020) 1901973, https://doi.org/10.1002/AENM.201901973.
[57] A.A.A. Ahmed, Z.A. Talib, M.Z. Bin Hussein, A. Zakaria, Zn-Al layered double hydroxide prepared at different molar ratios: preparation, characterization, optical and dielectric properties, J. Solid State Chem. 191 (2012) 271–278, https://doi.org/10.1016/j.jssc.2012.03.013.
[58] L. Mohapatra, K. Parida, A review on the recent progress, challenges and perspective of layered double hydroxides as promising photocatalysts, J. Mater. Chem. A 4 (2016) 10744–10766, https://doi.org/10.1039/c6ta01668e.
[59] S. Kim, J. Fahel, P. Durand, E. André, C. Carteret, Ternary Layered Double Hydroxides (LDHs) Based on Co-, Cu-Substituted ZnAl for the Design of Efficient Photocatalysts, Eur. J. Inorg. Chem. 2017 (2017) 669–678, https://doi.org/10.1002/ejic.201601213.
[60] B. Van Den Bogaert, L. Gheeraert, M.E. Leblebici, K. Binnemans, T. Van Gerven, Photochemical recovery of europium from non-aqueous solutions, PCCP 18 (2016) 29961–29968, https://doi.org/10.1039/C6CP06329B.
[61] Y. Chen, F. Li, G. Yu, X. Yang, Fluorescence of Zn-Al-Eu ternary layered hydroxide response to phenylalanine, Spectrochim. Acta - Part A Mol, Biomol. Spectrosc. 86 (2012) 625–630, https://doi.org/10.1016/j.saa.2011.11.029.
[62] A.C. Teixeira, I.G. Nunes Silva, A.F. Morais, D. Mustafa, Structural and optical properties of pillared Eu3+-containing layered double hydroxides intercalated by 2- to 12-carbon aliphatic dicarboxylates, J. Rare Earths 40 (2022) 260–267, https://doi.org/10.1016/j.jre.2020.10.023.
[63] X. Xiong, Y. Zhao, R. Shi, W. Yin, Y. Zhao, G.I.N. Waterhouse, T. Zhang, Selective photocatalytic CO_2 reduction over Zn-based layered double hydroxides containing tri or tetravalent metals, Sci. Bull. 65 (2020) 987–994, https://doi.org/10.1016/j.scib.2020.03.032.
[64] X. She, J. Wu, H. Xu, J. Zhong, Y. Wang, Y. Song, K. Nie, Y. Liu, Y. Yang, M.-T.-F. Rodrigues, R. Vajtai, J. Lou, D. Du, H. Li, P.M. Ajayan, X. She, H. Xu, D. Du, H. Li, J. Wu, Y. Wang, Y. Song, Y. Liu, Y. Yang, M.F. Rodrigues, R. Vajtai, J. Lou, P. M. Ajayan, J. Zhong, K. Nie, High Efficiency Photocatalytic Water Splitting Using 2D α-Fe_2O_3/g-C_3N_4 Z-Scheme Catalysts, Adv. Energy Mater. 7 (2017) 1700025, https://doi.org/10.1002/AENM.201700025.

[65] S.M. Xu, T. Pan, Y.B. Dou, H. Yan, S.T. Zhang, F.Y. Ning, W.Y. Shi, M. Wei, Theoretical and Experimental Study on $M^{II}M^{III}$-Layered Double Hydroxides as Efficient Photocatalysts toward Oxygen Evolution from Water, J. Phys. Chem. C 119 (2015) 18823–18834, https://doi.org/10.1021/acs.jpcc.5b01819.

[66] M.J. Wu, J.Z. Wu, J. Zhang, H. Chen, J.Z. Zhou, G.R. Qian, Z.P. Xu, Z. Du, Q.L. Rao, A review on fabricating heterostructures from layered double hydroxides for enhanced photocatalytic activities, Catal, Sci. Technol. 8 (2018) 1207–1228, https://doi.org/10.1039/c7cy02314f.

[67] J. Zhao, Y. Lu, D. Wu, Y. Qin, Y. Xie, Y. Guo, W. Raza, G. Luo, M. Asim Mushtaq, Y. Wu, X. Mu, Y. Ling, T. Ilyas, Q. Ul Hassan, C. Gao, Regulating divalent metal species in aluminum-based layered double hydroxides to selectively promote photocatalytic CO production from CO_2, Sep. Purif. Technol. 305 (2023), 122508, https://doi.org/10.1016/J.SEPPUR.2022.122508.

[68] B. Lin, P. Sun, Y. Zhou, S. Jiang, B. Gao, Y. Chen, Interstratified nanohybrid assembled by alternating cationic layered double hydroxide nanosheets and anionic layered titanate nanosheets with superior photocatalytic activity, J. Hazard. Mater. 280 (2014) 156–163, https://doi.org/10.1016/J.JHAZMAT.2014.07.068.

[69] X. Zhang, L. Wang, X. Zhou, Z. Ni, S. Xia, Investigation into the Enhancement of Property and the Difference of Mechanism on Visible Light Degradation of Gaseous Toluene Catalyzed by ZnAl Layered Double Hydroxides before and after Au Support, ACS Sustain. Chem. Eng. 6 (2018) 13395–13407, https://doi.org/10.1021/acssuschemeng.8b03186.

[70] A. Nehdi, N. Frini-Srasra, G. de Miguel, I. Pavlovic, L. Sánchez, J. Fragoso, Use of LDH- chromate adsorption co-product as an air purification photocatalyst, Chemosphere 286 (2022), https://doi.org/10.1016/j.chemosphere.2021.131812.

[71] M. Cruz-Yusta M. Sánchez L. Sánchez Metal Oxide Nanomaterials for Nitrogen Oxides Removal in Urban Environments D. Barreca C. Maccato Tailored Funct 2022 Oxide Nanomater., Wiley 229 276 10.1002/9783527826940.ch7.

[72] H. Li, H. Zhu, Y. Shi, H. Shang, L. Zhang, J. Wang, Vacancy-Rich and Porous NiFe-Layered Double Hydroxide Ultrathin Nanosheets for Efficient Photocatalytic NO Oxidation and Storage, Environ. Sci. Tech. 56 (2022) 1771–1779, https://doi.org/10.1021/acs.est.1c07811.

[73] R.J. Lewis, N.I. Sax, Sax's Dangerous Properties of Industrial Materials, twelfth, Wiley, New York, 2004. doi:10.1002/0471701343.

[74] H. Khan, M. Gar Alalm, M. Lalonde-Lavoie, M.F. Ordonez, M. Sartirana, A. Giordana, G. Cerrato, C.L. Bianchi, D.C. Boffito, Photocatalytic degradation of NOx and ethanol in the gas phase by spray dried Ce-TiO_2, J. Environ. Chem. Eng. 9 (6) (2021), https://doi.org/10.1016/J.JECE.2021.106813.

[75] Q. Zhu, R. Hailili, Y. Xin, Y. Zhou, Y. Huang, X. Pang, K. Zhang, P.K.J. Robertson, D.W. Bahnemann, C. Wang, Efficient full spectrum responsive photocatalytic NO conversion at $Bi_2Ti_2O_7$: Co-effect of plasmonic Bi and oxygen vacancies, Appl. Catal. B Environ. 319 (2022), 121888, https://doi.org/10.1016/j.apcatb.2022.121888.

[76] F. Chang, Z. Wei, Z. Zhao, Y. Qi, D. guo, Liu, 2D–2D heterostructured composites Bi_4O_5Br 2-Sn_S2 with boosted photocatalytic NOx abatement, J. Ind. Eng. Chem. 117 (2023) 265–272, https://doi.org/10.1016/J.JIEC.2022.10.015.

[77] B. Xie, D. Chen, N. Li, Q. Xu, H. Li, J. Lu, Lead-Free Cs_3Bi_2Br 9 perovskite In-situ growth on 3D Flower-like g-$_C3_N$4 microspheres to improve photocatalytic performance, Chem. Eng. J. 452 (2023), 139662, https://doi.org/10.1016/j.cej.2022.139662.

[78] K. Qi, J. Jing, G. Dong, P. Li, Y. Huang, The excellent photocatalytic NO removal performance relates to the synergistic effect between the prepositive NaOH solution and the g-C_3N_4 photocatalysis, Environ. Res. 212 (2022), 113405, https://doi.org/10.1016/J.ENVRES.2022.113405.

[79] M. Fu, X. Hu, C. Wang, P. Lu, J. Bai, R. Wang, X. Tan, Constructing a novel $NaLa(WO_4)_2$/g-C_3N_4 Z-scheme heterojunction with efficient carrier separation for excellent photocatalytic purification of NO, J. Alloy. Compd. 906 (2022), 164371, https://doi.org/10.1016/J.JALLCOM.2022.164371.

[80] A. De Roy, C. Forano, J.P. Besse, Layered double hydroxides: synthesis and post-synthesis modification, in: V. Rives (Ed.), Layer. Double Hydroxides Present Futur., Nova Science Publishers Inc, New York, 2001: pp. 1–39.

[81] Z. Zhang, G. Chen, K. Xu, Photoluminescence of Colloids of Pristine ZnAl Layered Double Hydroxides, Ind. Eng. Chem. Res. 52 (2013) 11045–11049, https://doi.org/10.1021/ie4012326.

[82] A.F. Morais, D. Nanclares, I.G.N. Silva, A. Duarte, F.A. Garcia, E. Breynaert, D. Mustafa, Mesostructuring layered materials: Self-supported mesoporous layered double hydroxide nanotubes, Nanoscale 13 (2021) 11781–11792, https://doi.org/10.1039/d1nr02477a.

[83] A.F. Morais, I.G.N. Silva, B.C. Lima, F.A. Garcia, D. Mustafa, Coordination of Eu^{3+} Activators in ZnAlEu Layered Double Hydroxides Intercalated by Isophthalate and Nitrilotriacetate, ACS Omega 5 (2020) 23778–23785, https://doi.org/10.1021/acsomega.0c02848.

[84] T. Stumpf, H. Curtius, C. Walther, K. Dardenne, K. Ufer, T. Fanghänel, Incorporation of Eu(III) into Hydrotalcite: A TRLFS and EXAFS Study, Environ. Sci. Tech. 41 (2007) 3186–3191, https://doi.org/10.1021/es0624873.

[85] M. Wang, C. Huang, Z. Huang, W. Guo, J. Huang, H. He, H. Wang, Y. Cao, Q. Liu, J. Liang, Synthesis and photoluminescence of Eu-doped ZnO microrods prepared by hydrothermal method, Opt. Mater. (Amst) 31 (2009) 1502–1505, https://doi.org/10.1016/J.OPTMAT.2009.02.009.

[86] I.G.N. Silva, D. Mustafa, B. Andreoli, M.C.F.C. Felinto, O.L. Malta, H.F. Brito, Highly luminescent Eu^{3+}-doped benzenetricarboxylate based materials, J. Lumin. 170 (2016) 364–368, https://doi.org/10.1016/J.JLUMIN.2015.04.047.

[87] I.G.N. Silva, A.F. Morais, B.C. Lima, F.A. Garcia, D. Mustafa, Investigation of the structure-luminescence relationship in ZnAlEu layered double hydroxides intercalated with nitrate and benzenecarboxylates, Appl. Clay Sci. 199 (2020), 105861, https://doi.org/10.1016/j.clay.2020.105861.

[88] T. Jin, S. Tsutsumi, Y. Deguchi, K. Machida, G. Adachi, Preparation and luminescence characteristics of the europium and terbium complexes incorporated into a silica matrix using a sol–gel method, J. Alloy. Compd. 252 (1997) 59–66, https://doi.org/10.1016/S0925-8388(96)02385-7.

[89] D. Dvoranová, Z. Barbieriková, V. Brezová, Radical intermediates in photoinduced reactions on TiO_2 (An EPR spin trapping study), Molecules 19 (2014) 17279–17304, https://doi.org/10.3390/molecules191117279.